Available online at www.sciencedirect.com
SCIENCE DIRECT
Journal of the European Ceramic Society 26 (2006) 417–422
www.elsevier.com/locate/jeurceramsoc

Synthesis, characterization and sinterablity of 10 mol% Sm_2O_3-doped CeO_2 nanopowders via carbonate precipitation

Yarong Wang [a,*], Toshiyuki Mori [a], Ji-Guang Li [b], Yoshiyuki Yajima [b], John Drennan [c]

[a] *Ecomaterials Center, National Institute for Materials Science, Namiki 1-1, Tsukuba, Ibaraki 305-0044, Japan*
[b] *Advanced Materials Laboratory, National Institute for Materials Science, Namiki 1-1, Tsukuba, Ibaraki 305-0044, Japan*
[c] *Centre for Microscopy and Microanalysis, The University of Qeensland, St. Lucia, Brisbane, Qld 4072, Australia*

Available online 10 August 2005

Abstract

A carbonate coprecipitation method has been used for the facile synthesis of highly reactive 10 mol% Sm_2O_3-doped CeO_2 (20SDC) nanopowders, employing nitrates as the starting salts and ammonium hydrogen carbonate (AHC) as the precipitant. The AHC/RE^{3+} (RE = Ce + Sm) molar ratio (R) and the reaction temperature (T) affect significantly the final yield and precursor properties, including chemical composition and particle morphology. Suitable processing conditions are $T = 60\,^{\circ}C$ and $R = 5.0$–10, under which precipitation is complete and the resultant precursors show ultrafine particle size, spherical particle shape, and good dispersion. Thus, the processed precursors are rare-earth carbonates with an approximate formula of $Ce_{0.8}Sm_{0.2}(CO_3)_{1.5}{\cdot}1.8H_2O$, which directly yield oxide solid-solutions upon thermal decomposition at a low temperature of $\sim$440 °C. The 20SDC solid solution powders calcined at 700 °C show excellent reactivity and have been densified to $\sim$99% of the theoretical via pressureless sintering at a very low temperature of 1200 °C for 4 h.

Keywords: Powders-chemical preparation; Sintering; CeO_2; Fuel cells

1. Introduction

Ceria (CeO_2) is a fluorite-structured oxide that forms extensive solid solutions with a variety of alien cations. With aliovalent (alkaline-earth or rare-earth) dopants, oxygen vacancies are created in the CeO_2 lattice for charge compensation, and the resultant oxide solid-solutions are valuable for applications as an oxygen buffer in the automotive three-way catalysts (TWCs), as a promoter for gas phase oxidation/reduction reactions, and as solid electrolytes or anodes in intermediate-temperature solid oxide fuel cells (SOFCs).[1] Among doped ceria materials, the Sm_2O_3/CeO_2 system (SDC) shows the highest electrical conductivity at a fixed doping level, since Sm^{3+}-doping induces the least distortion of the parent lattice.[2]

Traditionally, dense ceria-based electrolytes were fabricated via solid-state reaction by heat-treating a mixture of the individual component oxide powders at $\sim$1300 °C to yield a single phase solid-solution and subsequently refiring the solid-solution powder at even higher temperatures of $\sim$1700–1800 °C.[3,4] To reduce the densification temperature, a handful of wet-chemical processing techniques have been developed for SDC synthesis during recent years, typically oxalate coprecipitation[5,6] and hydrothermal treatment.[7]

The properties of a wet-chemically derived oxide powder are known to heavily depend upon the characteristics of its precursor, exhibiting the existence of some sort of "genetic" relationship. Carbonates may serve as excellent precursors for highly sinterable oxides,[8,9] since carbonates, unlike most hydroxides, are non-gelatinous and show much weaker agglomeration after drying. The carbonate coprecipitation method is especially effective for the synthesis of rare-earth doped CeO_2 nanopowders, as rare-earth cations readily form carbonate solid solutions,[10] which allows intimate (atomic level) mixing of the cations in the precursor and hence low-temperature formation of the aimed phase. Carbonate coprecipitation can be achieved with a variety of water-soluble carbonate salts as the precipitant, among

* Corresponding author. Tel.: +81 29 851 3354x8540; fax: +81 29 852 7449.
E-mail address: WANG.Yarong@nims.go.jp (Y. Wang).

0955-2219/$ – see front matter © 2005 Elsevier Ltd. All rights reserved.
doi:10.1016/j.jeurceramsoc.2005.07.028

which ammonium hydrogen carbonate and ammonium carbonate are preferred, as they do not introduce impurity cations into the final product. The purpose of this work is to synthesize 10 mol% Sm_2O_3-doped CeO_2 (20SDC) nanopowders via carbonate coprecipitation with ammonium hydrogen carbonate as the precipitant. Through optimizing synthetic conditions, highly reactive 20SDC powders, which can be densified to ~99% of the theoretical, have been obtained. In the following sections, we report the powder synthesis, characterization, and the ceramics fabrication.

2. Experimental procedure

2.1. Powder synthesis

The starting materials for 20SDC synthesis are cerium and samarium nitrate hexahydrate ($RE(NO_3)_3{\cdot}6H_2O$, >99.95% pure, RE = Ce and Sm) and ammonium hydrogen carbonate (NH_4HCO_3, ultrahigh purity, hereafter referred to as ammonium hydrogen carbonate (AHC)). The chemicals were all purchased from Kanto Chemical Co., Inc. (Tokyo, Japan) and were used as received without further purification.

For precursor synthesis, 250 mL of the mixed salt solution (0.08 M Ce^{3+} + 0.02 M Sm^{3+}) was dripped into an equivolume of the precipitant solution kept at selected temperatures under mild stirring. After aging at the reaction temperature for 1 h, the resultant suspension was filtered via suction filtration. After repeated washing with distilled water and final rinsing with anhydrous ethanol, the precipitate cake was dried at room temperature under flowing nitrogen gas and then lightly pulverized with a zirconia mortar and pestle before calcining to yield oxide powders. Calcination of the carbonate precursors were performed under flowing O_2 gas (50 mL/min) in a tube furnace, using a heating rate of 5 °C/min and a residence time of 2 h at the selected temperatures.

2.2. Powder characterization

Composition of the precursor was determined by chemical analysis. Cation contents were analyzed by the ICP spectrophotometric method with an accuracy of 0.01 wt.%; carbon content was assayed on a simultaneous carbon/sulfur determinator with a detection limit of 0.01 wt.% (Model CS-444LS, LECO, St. Joseph, MI, U.S.A.); NH_4^+ content was determined by the distillation-titrimetric method with an experimental error of ± 0.1 wt.%.

Differential thermal analysis/thermogravimetry (DTA/TG) of the dried precursor is made on a TG-DTA analyzer (EXSTASR6200, SEIKO, Tokyo, Japan) in stagnant air with a heating rate of 10 °C/min, using platinum crucible as the sample container and alpha-alumina as the reference.

Phase identification is performed via X-ray diffractometry (XRD) on a Rigaku RINT 2200HF$^+$ Ultima$^+$ X-ray diffractometer (Rigaku, Tokyo, Japan) operating at 40 kV/40 mA using monochromatized Cu Kα radiation. Diffractions are recorded by continuous scanning with a speed of 1° 2θ/min. Lattice parameter of the 20SDC solid solution is calculated with the LCR2 program.[11]

Particle morphology and agglomeration state of the synthesized powders were observed via field-emission scanning electron microscopy (FESEM, Model S-5000, Hitachi, Tokyo, Japan), after ultrasonic dispersing, drying, and osmium coating (for better conductivity).

2.3. Sintering

Sintering of the powders was performed in air after cold isostatic compaction at 300 MPa pressure. Microstructure of the sintered body was observed via FESEM after polishing, thermal etching, and Os coating.

3. Results and discussion

3.1. The effects of reaction temperature on precursor morphology

Reaction temperature has substantial effects on the precursor morphology, and a higher temperature tends to prevent the formation of hard aggregates. Fig. 1 shows morphologies of the precursor particles processed at [AHC] = 0.5 M [AHC/(Ce^{3+} + Sm^{3+}) molar ratio R = 5] for two typical reaction temperatures. The powder prepared at room temperature contains a large amount of big plate-like particles as well as fine spherical particles (Fig. 1a). EDX analysis, though not given here, show that the two types of particles possess almost identical Ce and Sm contents, implying that the plate-like particles are likely hard aggregates of primary particles rather than a different phase. The plate-like particles were significantly reduced in amount by raising the reaction temperature to 40 °C, at which they are only occasionally observed. The plate-like particle was no longer observed in the powder prepared at 60 °C, and the precursor solely contains fine spherical particles, which loosely agglomerate to form porous networks (Fig. 1b). Even higher reaction temperatures are not tried due to the ease of AHC decomposition. Similar dependence of particle morphology on the reaction temperature was also observed at other R values.

3.2. The effects of AHC/RE^{3+} molar ratio (R) on precursor properties

At the optimal reaction temperature of 60 °C, we have also investigated the influences of AHC concentration (the R value) on precursor composition, particle morphology, and the completeness of precipitation.

Fig. 2 shows XRD patterns of the as-dried 20SDC precursors. All the powders show low crystallinity, making it difficult to perform phase identification and composition determination via XRD analysis. Obviously, the AHC concentration (i.e. the R value) affects the properties of the

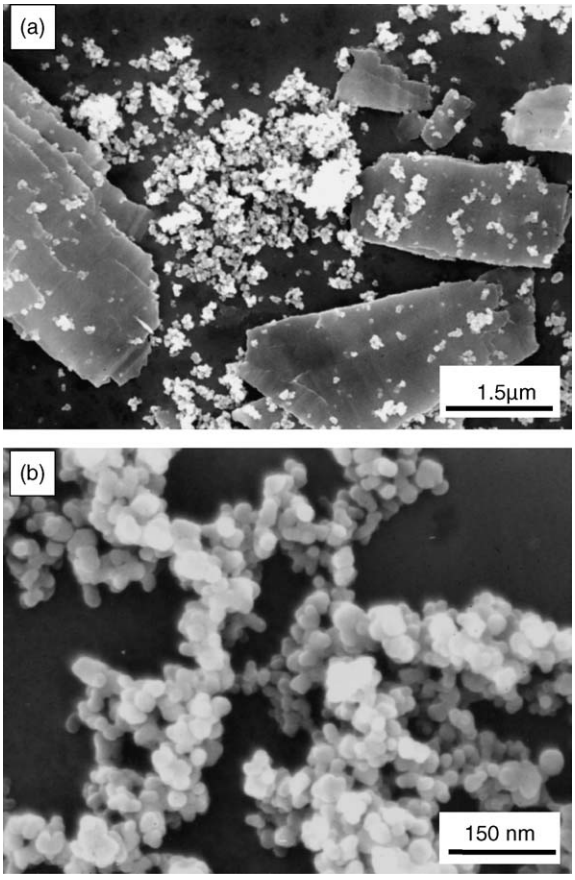

Fig. 1. FESEM micrographs showing particle morphologies of the powders processed at different reaction temperatures: (a) room temperature and (b) 60 °C.

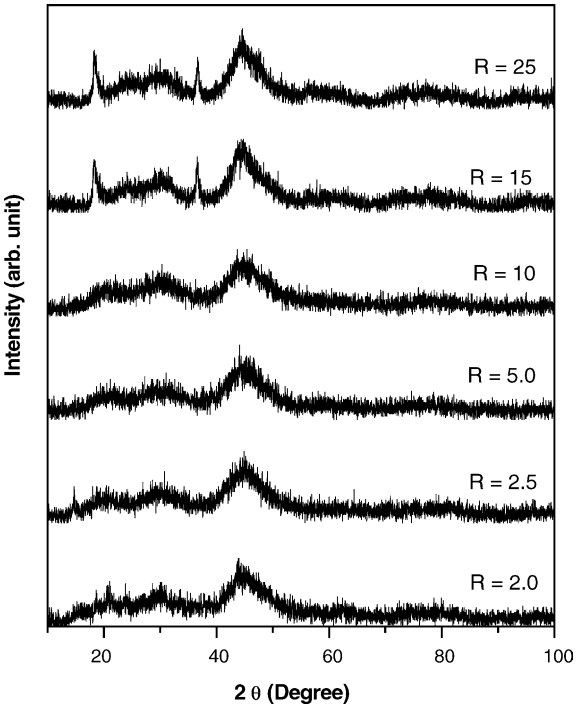

Fig. 2. XRD patterns of the precursors synthesized at various R values (R = AHC/RE^{3+} molar ratio) at a fixed temperature of 60 °C.

Table 1
Elemental contents (wt.%) of the precursors processed at 60 °C

R	Ce	Sm	C	NH_4^+	Ce:Sm:C:NH_4^+ molar ratio
25	42.8	11.9	7.16	0.93	0.8:0.21:1.57:0.14
15	41.4	11.4	6.85	0.83	0.8:0.21:1.54:0.12
10	43.7	11.6	6.57	0.49	0.8:0.20:1.40:0.06
5.0	43.4	11.9	6.55	0.30	0.8:0.20:1.41:0.04
2.5	41.3	12.0	6.07	0.12	0.8:0.22:1.38:0.02
2.0	42.7	12.7	6.46	N.D.	0.8:0.22:1.41

N.D.: not detected positively at a detection limit of 0.1 wt.%.

resultant precursors. The two additional peaks (at diffraction angle $2\theta \approx 18.28°$ and 36.59°, respectively) observed in the XRD patterns of the precursors obtained at $R = 15$ and 25 are absent in the patterns of those obtained at lower R values, indicating partial crystallization of the two precursors.

Elemental analysis (Table 1) shows that the precursors, in the studied range ($2.0 \leq R \leq 25$), are stoichiometric within the accuracy of the analysis method (±0.01 wt.%), indicating the occurrence of quantitative precipitation. All the samples contain considerable amounts of C (from CO_3^{2-}) and are free of NO_3^-, indicating that the precursors are primarily carbonates and that NO_3^- is non-precipitating. Besides, the powders obtained at $R \leq 10$ are almost free of NH_4^+, which is in contrast to those synthesized at higher R values. Based on the results of elemental analysis and considering molecular electrical neutrality as well as the weight loss in thermal decomposition (which will be discuss in detail in Section 3.3), the precursors prepared at $2.0 \leq R \leq 10$ are normal carbonates possessing an approximate formulae of $Ce_{0.8}Sm_{0.2}(CO_3)_{1.5}\cdot 1.8H_2O$. NH_4^+ contents of the samples processed at $R > 10$ increased significantly, mainly due to the increased complexation of RE^{3+} cations with NH_4^+. NH_4^+ is known to complex rare-earth cations, and the extent of complexation increases along with an increase in the NH_4^+ concentration.[12] The samples made at $R > 10$ possess a general chemical formulae of $(NH_4)_xCe_{0.8}Sm_{0.2}(CO_3)_{1.5+x/2}\cdot 1.4H_2O$, where the x value increases from ~0.12 at $R = 15.0$ to ~0.14 at $R = 25$.

Fig. 3 shows particle morphologies of the precursors processed at two typical R values. The precursor obtained at $R = 25$ contains rod-like particles of ~30 nm in diameter and ~0.2 mm in length (Fig. 3a). At $R = 15$, the precursor is still mainly composed of rod-like particles, but in shorter length. When the R ratio is reduced to 10, the precursor mainly contains rounded primary particles, with only very few short rod-like particles observed. The precursors obtained at $R < 10$ are exclusively composed of spherical particles, as is shown in Fig. 3b for that made at $R = 5$.

The extent of precipitation has also been investigated by analyzing the RE cations that remain in the filtrate after precipitation. Nearly complete precipitation is achieved in the range $5.0 \leq R \leq 10$ (the RE cations remained in the filtrate are below the detection limit of ICP). Beyond this range, however, considerable amounts of RE cations are left in the filtrate after precipitation. It is observed that the filtrate at

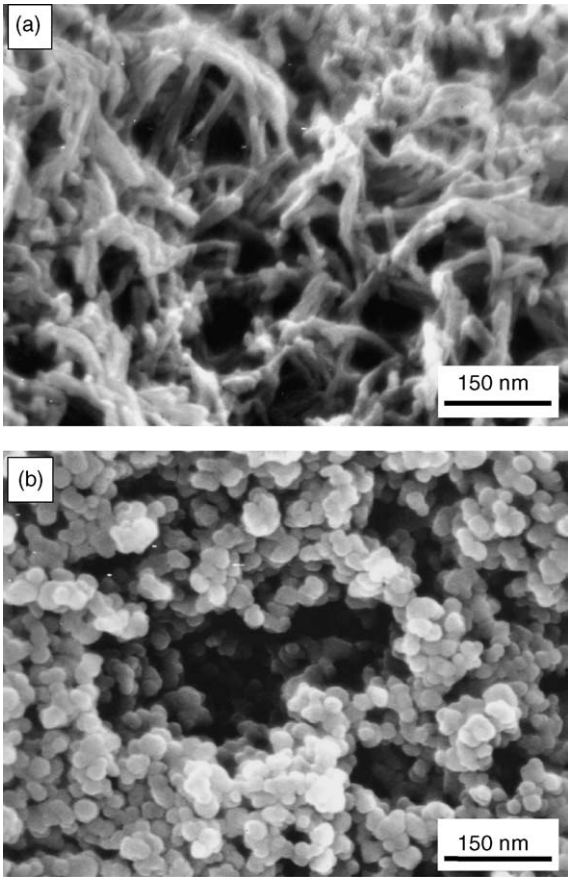

Fig. 3. FESEM micrographs showing particle morphologies of the powders processed at 60 °C with different R values: (a) $R = 25$ and (b) $R = 2.0$.

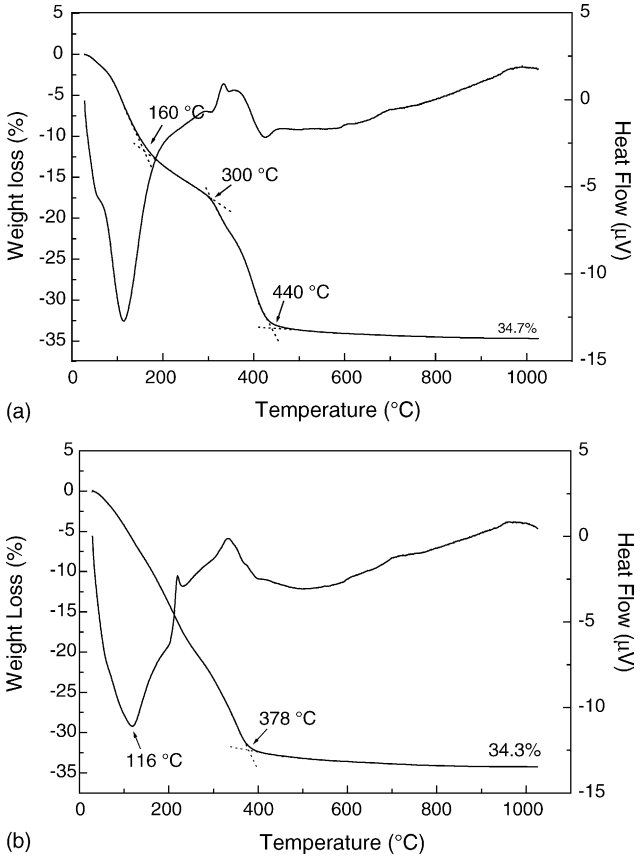

Fig. 4. DTA/TG curves of the precursors synthesized at (a) $R = 5$ and (b) $R = 25$. The data were taken in stagnant air at a heating rate of 10 °C/min.

$R = 2.0$ is colorless while those at $R > 10$ have a yellow color, which gradually thickens at a higher R value. The incomplete precipitation at $R < 5.0$ is due to the inadequacy of precipitant, which is evidenced by the low pH value (~5.9) of the precipitation system (pH ~ 8.1 for $R \geq 5.0$). On the other hand, the incompleteness at $R > 10$ was considered to be mainly due to the formation of stable RE^{3+}/NH^{4+} complexes.[12] The precipitation yields at $R = 2.0$, 2.5, 15 and 25 are ~85, 91, 98 and 95%, respectively, as determined from the weights of the resultant solid solution oxides.

3.3. Thermal decomposition behavior of the precursor and morphologies of the resultant oxide solid solutions

Typical decomposition behaviors of the carbonate precursors synthesized in this work are shown in Fig. 4. The normal carbonate precursors obtained at $R \leq 10$ decompose to oxide via three distinct stages (Fig. 4a). The first stage, mainly occurring at temperatures up to ~160 °C, is due to the evaporation of the absorbed moisture and the release of molecular water. The calculated weight loss (~12.3%) for this stage agrees with the value (~11.9%) revealed by TG at ~160 °C. The second stage, occurring in the range ~180–300 °C, may correspond to the partial decomposition of $Ce_{0.8}Sm_{0.2}(CO_3)_{1.5}$ to yield oxycarbonate intermediates.[13] The weight loss at even higher temperatures (the third stage) is due to the further decomposition of the oxycarbonate to yield oxide. Complete decomposition is almost achieved at ~440 °C. The final ignition loss (~34.7%) is also in accordance with that (~34.8%) calculated from the complete decomposition of $Ce_{0.8}Sm_{0.2}(CO_3)_{1.5}\cdot 1.8H_2O$. The broad and weak exothermic peak in the range ~300–400 °C may correspond to the oxidation of Ce^{3+} to Ce^{4+} cations. The ammonium rare-earth carbonate precursors obtained at $R > 10$ show weaker thermal events on the DTA curve and exhibits a slightly lower decomposition temperature, as is shown in Fig. 4b for the precursor made at $R = 25$. The decomposition is almost completed at ~378 °C, and the final weight loss 34.3% also agree well with that (34.7%) calculated from the complete decomposition of $(NH_4)_{0.14}Ce_{0.8}Sm_{0.2}(CO_3)_{1.57}\cdot 1.4H_2O$.

As only the normal carbonates prepared at $R \leq 10$ show morphologies beneficial to the generation of dispersed spherical oxide particles via thermal decomposition, more detailed characterizations on the phase evolution was made using the precursor synthesized at $R = 5$ and 60 °C as a representative.

Fig. 5 shows XRD patterns of the 20SDC powders calcined at various temperatures for 2 h. Crystallization of the powder occurs at a minimum temperature of 300 °C and major diffraction peaks corresponding to the fluorite-structure of

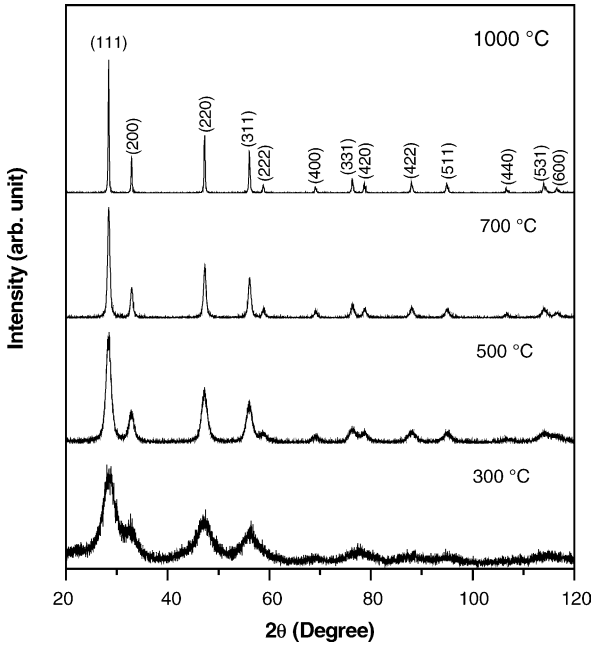

Fig. 5. XRD patterns of the 20SDC powders calcined under flowing O_2 gas at various temperatures for 2 h. The powders are from the precursor prepared at $R = 5$ and $T = 60\,^{\circ}C$.

CeO_2 (JCPDS: 34–394) have appeared. Apparently, oxidation of Ce^{3+} cations to Ce^{4+} has occurred up to 300 °C during calcination. The oxidation temperature is lower than that observed on the DTA curve (Fig. 4a), but is understandable by considering the different atmospheres (stagnant air for DTA/TG and pure O_2 for calcination) and the different residence time (no holding during DTA/TG analysis). Continuous refinements in peak shapes and intensities were observed along with an increase in the calcination temperature, indicating crystallite growth. Crystalline phase corresponding to Sm_2O_3 was not found at any calcination temperature, suggesting an intimate mixing of Ce^{3+} and Sm^{3+} cations in the precursor and the direct formation of oxide solid solution. Indeed, lanthanides readily form carbonate or hydroxyl carbonate solid-solutions among each other,[10] due to their similar chemical properties. The lattice parameter of the 20SDC oxide calcined at 1000 °C was determined to be $a = 0.54340 \pm 0.00002$ nm, using a computer program based on the Rietveld method. Apparently, Sm^{3+} doping induces an expansion in the unit cell of CeO_2 ($a = 0.541134(12)$ nm). Assuming that the Sm^{3+} cations are homogeneously distributed in the CeO_2 lattice and occupy the Ce^{4+} sites to form a solid-solution of $Ce_{0.8}Sm_{0.2}O_{1.9}$, X-ray density of the 20SDC solid-solution, d_{th}, was calculated to be 7.146 g/cm^3 according to the following equation

$$d_{th} = 4\frac{(1-x)M_{Ce} + xM_{Sm} + (2-x/2)M_O}{a^3 N_A}, \quad (1)$$

where $x = 0.2$ in this work, a is the lattice constant of the solid solution at room temperature, N_A is the Avogadro constant, and M denotes the atomic weight.

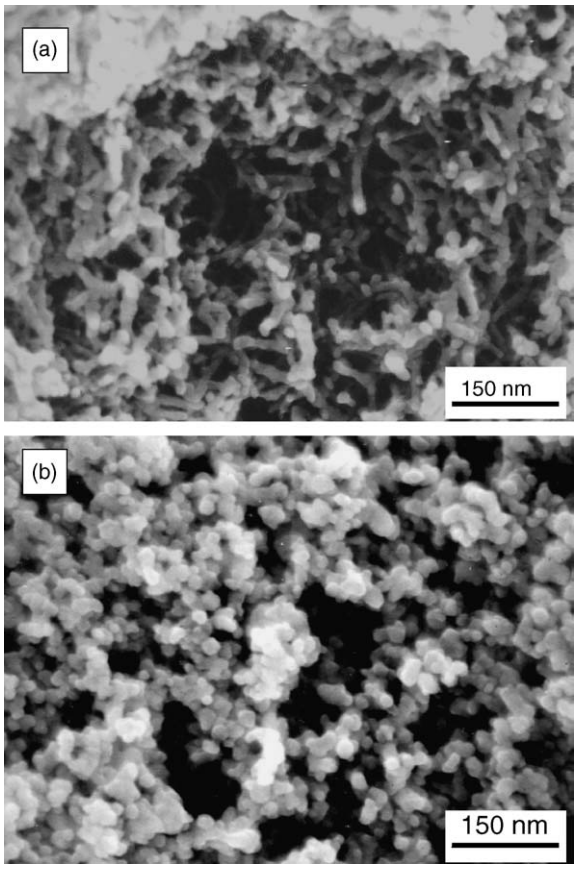

Fig. 6. FESEM micrographs showing particle morphologies of the powders calcined at 700 °C for 2 h from: (a) the precursor prepared at $R = 25$ and (b) the precursor prepared at $R = 5.0$.

Particle morphologies of the resultant solid-solution oxides clearly depend upon those of their respective precursors. Fig. 6 shows morphologies of the powders calcined at 700 °C for 2 h from the precursors prepared under 60 °C and at $R = 25$ and 5.0, respectively. The powder from the precursor prepared at $R = 25$ is still composed of rod-like particles after the calcination, though the rods are thinner and shorter than those in the precursor (Fig. 6a). The powder from the precursor made at $R = 15$ contains even shorter rods, while those from the precursors synthesized at $R \leq 10$ only contain well-dispersed fine spherical particles (Fig. 6b). Crystallite size of the powder shown in Fig. 6b was assayed to be 15.2 nm from the Scherrer equation via X-ray line broadening analysis performed on the (4 2 2) diffraction, which is close to that observed from the FESEM image.

The powder shown in Fig. 6b possesses excellent sintering reactivity. After dry isostatic compaction at 300 MPa, which yield a relative green density of ~51.7%, nearly fully dense 20SDC ceramics have been fabricated from the powder via pressureless sintering at a quite low temperature of 1200 °C for 4 h. Fig. 7 shows microstructure of the densified ceramic, from which the average grain size was calculated to be ~0.23 μm by the linear intercept method. Relative density of the ceramic is ~99% of the theoreti-

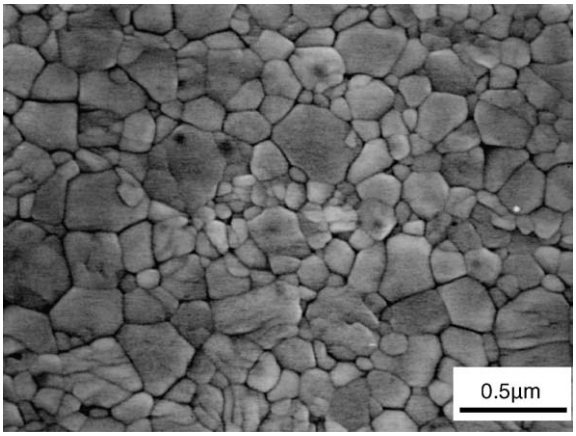

Fig. 7. FESEM micrograph showing microstructure of the 20SDC ceramic sintered at 1200 °C for 4 h using the powder shown in Fig. 6b. The sample surfaces were polished to 1-μm finish with diamond paste and then thermally etched at 1100 °C for 1 h to reveal grain boundaries.

cal, as determined by the Archimedes method using distilled water as an intrusion medium. The powders calcined at lower temperatures possess finer crystallite sizes, but are difficult to consolidate into green bodies of reasonable density by the dry compaction method used in this work, due to the greatly enhanced friction forces among the finer crystallites. Besides, the green compacts frequently crack upon sintering, because of the internal stresses caused by rapid shrinkage. Higher calcination temperature, on the other hand, lowers the sinterability due to the increased crystallite size. The densification temperature achieved in this work is significantly lower than the previously reported ones, typically $\geq$1700 °C[3,4] for the powders obtained via solid state reaction and ~1400–1600 °C for the powders processed via other wet chemical routes (such as oxalate coprecipitation[5,6] and hydrothermal treatment).[7] The preferred particle morphologies for low-temperature densification include ultrafine particle/crystallite size, less aggregation, and nearly spherical particle shape, as were shown in Fig. 6b. The powders made via solid-state reaction lack all of these powder characteristics. The wet-chemical routes mentioned above yield primary crystallites of nano dimension, but the crystallites are hard aggregated to form secondary particles of much larger sizes (up to tens of microns) and irregular shapes.[5–7] Therefore, the powders, though show better reactivity than those via solid-state reaction, still require high sintering temperatures. The low sintering temperature achieved in this work makes it possible to fabricate dense 20SDC electrolytes with almost any type of sintering furnace, which is very advantageous from the view point of energy saving and the ease of fabrication. The excellent sinterability mainly comes from the ultrafine size and good dispersion of the primary crystallites (Fig. 6b).

4. Conclusions

Highly sinterable 20SDC powders have been synthesized via coprecipitation using AHC as the precipitant. Processing parameters were found to significantly affect the precursor properties and the final yields. The best results were obtained at a reaction temperature of 60 °C and AHC/RE molar ratios of 5.0–10, where nearly complete precipitation was achieved and the resultant precursor particles, having an approximate composition of $Ce_{0.8}Sm_{0.2}(CO_3)_{1.5}\cdot 1.8H_2O$, are ultrafine in size, spherical in shape, and well dispersed. DTA/TG analysis indicates that the carbonate precursor decomposes to oxide up to ~440 °C, while XRD analysis revealed the direct formation of oxide solid solutions. The 20SDC solid solution powders calcined at 700 °C show excellent reactivity and have been densified to ~99% of the theoretical via pressureless sintering at a very low temperature of 1200 °C for 4 h.

References

1. Minh, N. Q., Ceramic fuel cells. *J. Am. Ceram. Soc.*, 1993, **76**, 563–588.
2. Inaba, H. and Tagawa, H., Ceria-based solid electrolytes. *Solid State Ionics*, 1996, **83**, 1–16.
3. Yahiro, H., Eguchi, K. and Arai, H., Electrical properties and reducibilities of ceria-rare earth oxide systems and their application to solid oxide fuel cell. *Solid State Ionics*, 1989, **36**, 71–75.
4. Kudo, T. and Obayashi, H., Oxygen ion conduction of the fluorite-type $Ce_{1-x}Ln_xO_{2-x/2}$ (Ln: lanthanoid element). *J. Electrochem. Soc.*, 1975, **122**, 142–147.
5. Higashi, K., Sonoda, K., Ono, H., Sameshima, S. and Hirata, Y., Synthesis and sintering of rare-earth-doped ceria powder by the oxalate coprecipitation method. *J. Mater. Res.*, 1999, **14**, 957–967.
6. Duran, P., Moure, C. and Jurado, J. R., Sintering and microstructural development of ceria-gadolinia dispersed powders. *J. Mater. Sci.*, 1994, **29**, 1940–1948.
7. Yamashita, K., Ramanujachary, K. V. and Greenblatt, M., Hydrothermal synthesis and low temperature conduction properties of substituted ceria ceramics. *Solid State Ionics*, 1995, **81**, 53–60.
8. Wang, Y., Mori, T., Li, J.-G. and Ikegami, T., Low-temperature synthesis of praseodymium-doped ceria nanopowders. *J. Am. Ceram. Soc.*, 2002, **85**, 3105–3107.
9. Li, J.-G., Ikegami, T., Wang, Y. and Mori, T., Reactive ceria nanopowders via carbonate precipitation. *J. Am. Ceram. Soc.*, 2002, **85**, 2376–2378.
10. Wakita, H. and Kinoshita, S., A synthetic study of the solid solutions in the systems $La_2(CO_3)_3\cdot 8H_2O$-$Ce_2(CO_3)_3\cdot 8H_2O$ and $La(OH)CO_3$-$Ce(OH)CO_3$. *Bull. Chem. Soc. Jpn.*, 1979, **52**, 428–432.
11. Williams, D. E., *Lattice Constant Refinement*, Technical report no. IS-1052, Ames Laboratory, U.S.D.O.E., Iowa State University, Ames, IA, 1964.
12. Ryabchikov, D. I. and Terentyeva, E. A., In *Progress in the science and technology of the rare earth*, ed. L. Eyring. Pergamon Press, New York, 1964, p. 139.
13. Head, E. L. and Holley Jr., C. E., The preparation and thermal decomposition of some rare earth carbonates. In *Rare Earth Research II*, ed. K. S. Vorres. Gorden and Breach, London, 1964, pp. 51–63.